Energy Technology
Generation, Conversion, Storage, Distribution
www.entechnol.de

Improving CO_2 Separation Performance of MIL-53(Al) by Incorporating 1-*n*-Butyl-3-Methylimidazolium Methyl Sulfate

Harun Kulak, H. Mert Polat, Safiyye Kavak, Seda Keskin, and Alper Uzun**

1-*n*-Butyl-3-methylimidazolium methyl sulfate is incorporated into MIL-53(Al). Detailed characterization is done by X-ray fluorescence, Brunauer–Emmett–Teller surface area, scanning electron microscopy, X-ray diffraction, Fourier-transform infrared spectroscopy, and thermogravimetric analysis. Results show that ionic liquid (IL) interacts directly with the framework, significantly modifying the electronic environment of MIL-53(Al). Based on the volumetric gas adsorption measurements, CO_2, CH_4, and N_2 adsorption capacities decreased from 112.0, 46.4, and 19.6 cc (STP) $g_{MIL\text{-}53(Al)}^{-1}$ to 42.2, 13.0, and 4.3 cc (STP) $g_{MIL\text{-}53(Al)}^{-1}$ at 5 bar, respectively, upon IL incorporation. Data show that this postsynthesis modification leads to more than two and threefold increase in the ideal selectivity for CO_2 over CH_4 and N_2 separations, respectively, as compared with pristine MIL-53(Al). The isosteric heat of adsorption (Qst) values show that IL incorporation increases CO_2 affinity and decreases CH_4 and N_2 affinities. Cycling adsorption–desorption measurements show that the composite could be regenerated with almost no decrease in the CO_2 adsorption capacity for six cycles and confirm the lack of any significant IL leaching. The results offer MIL-53(Al) as an excellent platform for the development of a new class of IL/MOF composites with exceptional performance for CO_2 separation.

1. Introduction

CO_2 capture and separation is a major research subject as the current energy infrastructure strongly depends on fossil fuels. Due to the increasing atmospheric CO_2 concentration that triggers climate changes and global warming, there is a strong need for the development of effective technologies to reduce CO_2 emissions caused by burning of fossil fuels.[1] Not only removal of CO_2 from flue gases but also separation of CO_2 from natural gas is crucial because CO_2 decreases the energy density of natural gas and causes corrosion in the transport pipelines.[2] Current CO_2 separation technologies, cryogenic distillation and absorption, are energy-intensive processes.[3] Alternative separation technologies based on adsorption have been recently developed for efficient capturing of CO_2 from flue gas and upgrading of natural gas.[4] A diverse range of porous materials including activated carbons,[5] carbon nanotubes,[6] zeolites,[7] silica gels,[8] and carbon molecular sieves[9] have been utilized as adsorbents for the separation of CO_2.

Metal organic frameworks (MOFs) are a novel class of porous materials composed of metal ions connected by organic linkers,[10,11] and they have been considered as promising adsorbent materials for gas separation applications due to their wide range of pore sizes and shapes that can be suitable for the capture of specific gases.[12] MOFs have high pore volumes, very large surface areas, and versatile physical and chemical properties, which are important advantages compared with the conventional porous adsorbents.[12–14] Several studies show that desired adsorption selectivity for a specific gas separation can be achieved by designing new MOF materials.[15–18] However, this task-specific design approach requires tedious synthesis studies to discover such new materials with exceptionally high separation performance. Therefore, postsynthesis modification of an MOF, which offers high performance along with chemical and thermal stability, is a great opportunity for further improving its gas separation capacity. In this respect, using ionic liquids (ILs) for the postsynthesis modification of MOFs offers a broad potential. ILs are a class of salts consisting entirely of ions. They can be constituted of charged organic cations and organic or inorganic anions,

H. Kulak, Prof. S. Keskin, Prof. A. Uzun
Department of Chemical and Biological Engineering
Koç University
Rumelifeneri Yolu, 34450 Sariyer, Istanbul, Turkey
E-mail: skeskin@ku.edu.tr; auzun@ku.edu.tr

The ORCID identification number(s) for the author(s) of this article can be found under https://doi.org/10.1002/ente.201900157.

DOI: 10.1002/ente.201900157

H. Kulak, H. M. Polat, S. Kavak, Prof. S. Keskin, Prof. A. Uzun
Koç University TÜPRAŞ Energy Center (KUTEM)
Koç University
Rumelifeneri Yolu, 34450 Sariyer, Istanbul, Turkey

H. M. Polat, S. Kavak
Department of Materials Science and Engineering
Koç University
Rumelifeneri Yolu, 34450 Sariyer, Istanbul, Turkey

Prof. A. Uzun
Koç University Surface Science and Technology Center (KUYTAM)
Koç University
Rumelifeneri Yolu, 34450 Sariyer, Istanbul, Turkey

or neutral ion pairs. Because of their tunable physicochemical properties, they have been used in various applications, including synthesis,[19–21] catalysis,[22–24] gas storage and separation.[25–27] Modification of MOFs with ILs can be either by the incorporation of ILs into the framework[28–34] or coating the external surface area of MOFs with ILs forming a core-shell-like structure.[35]

Although these postsynthesis studies presented very promising results for the performance improvement of the parent MOFs in gas separation, very limited numbers of IL/MOF composites have been reported so far. Most of these studies focused on the two different types of MOFs, CuBTC,[32,34] and ZIF-8,[28,29,31,33,35] and there is currently a gap in the literature in terms of variety of MOFs used to make IL/MOF composites. Extending studies to different families of MOFs will provide a valuable insight into structural factors determining the performances of IL/MOF composites in gas storage and separation. Motivated from this point, we focused on the postsynthesis modification of MIL-53(Al), a widely studied MOF known to have a high selectivity toward CO_2,[15,36,37] with an IL. We incorporated 1-*n*-butyl-3-methylimidazolium methyl sulfate ([BMIM][$MeSO_4$]), a well-studied and commercially available IL, into MIL-53(Al). This halide-free alkyl sulfate IL was chosen because of its high CO_2 solubility,[38] thermal and chemical stability, and cost-effective synthesis, which make it possible to be applied to industrial processes.[39] The resulting structure was characterized in detail to elucidate the interactions between MIL-53(Al) and [BMIM][$MeSO_4$]. We then performed volumetric gas adsorption measurements on the pristine and [BMIM][$MeSO_4$]-incorporated MIL-53(Al) and examined CO_2/CH_4 and CO_2/N_2 selectivities to identify the effects of these interactions on the gas separation performance of materials. Data presented in this work illustrate that [BMIM][$MeSO_4$] incorporation increases the CO_2 selectivity by more than two-times, opening up new opportunities for IL/MOF composites.

2. Results and Discussion

After [BMIM][$MeSO_4$]/MIL-53(Al) composite was prepared, first the elemental analysis was performed to confirm the corresponding IL loading. X-ray fluorescence spectroscopy (XRF) results given in **Table 1** show that approximately 26 wt% of IL loading was achieved.

Based on the Brunauer–Emmett–Teller (BET) measurements, the surface area of pristine MIL-53(Al) was determined as 621.7 $m^2 g^{-1}$, whereas [BMIM][$MeSO_4$]/MIL-53(Al) has a significantly lower surface area of 47.2 $m^2 g^{-1}$. This decrease in the surface area is consistent with the decrease in N_2 adsorption amount upon IL incorporation into the framework (Figure S1, Supporting Information). Results also indicate a reduction in the pore volume of pristine MIL-53(Al) from 0.22 $cm^3 g^{-1}$ to an immeasurable value upon the deposition of IL. However, we note that BET results might be unreliable for [BMIM][$MeSO_4$]/MIL-53(Al) composite because of the low solubility of N_2 in the IL present inside the MOF, as the IL molecules might be located near the pore openings and might significantly block the accessibility of the pores under the conditions of BET measurements.[34]

Table 1. Elemental analysis results of pristine MIL-53(Al) and [BMIM][$MeSO_4$]/MIL-53(Al).

	Pristine MIL-53(Al)	[BMIM][$MeSO_4$]/MIL-53(Al)
Formula	Concentration [wt%]	Concentration [wt%]
CHN	86.4	88
Al	13.1	8.81
S	0.34	3.04
Impurities	0.16	0.15

Scanning electron microscopy (SEM) images obtained for the pristine MIL-53(Al) and the [BMIM][$MeSO_4$]/MIL-53(Al) composite are shown in **Figure 1**. In these images, crystallites having diameters between 2 and 6 μm were observed on pristine MIL-53(Al). Images further indicate that the particle size and morphology of the MIL-53(Al) do not change significantly upon the incorporation of [BMIM][$MeSO_4$].

The X-ray diffraction spectroscopy (XRD) patterns given in **Figure 2** show that characteristic features of MIL-53(Al) were preserved with some slight changes in intensities. These results confirm that the structure of the framework was conserved during the synthesis of the composite.[31–35] However, it is important to note that there are two peaks below 10° centered at 8.85° and 9.44°, indicating the large and narrow pore forms of MIL-53(Al), respectively.[40] Additional XRD analyses on [BMIM][$MeSO_4$]-incorporated MIL-53(Al) samples with a different IL loading illustrated that a higher loading of [BMIM][$MeSO_4$] induces a structural transformation from narrow to large pore by expanding the pores of MIL-53(Al) (Figure S3, Supporting Information). Thus, we infer that MIL-53(Al) in the composite material with 26 wt% IL loading, which we focus on in this study, has predominantly large pore configuration. Other observed intensity changes might be generated from either the change in crystal sizes depending on the sample preparation or a change in electronic environment as a consequence of the presence of the IL in the MOF structure. As these changes are connected with how IL molecules interact with the framework, we performed Fourier-transform infrared (FTIR) spectroscopy analysis and examined the changes in IR spectra to elucidate these interactions.

Figure 3 compares the IR spectrum of [BMIM][$MeSO_4$]/MIL-53(Al) composite with those of the pristine MIL-53(Al) and the bulk [BMIM][$MeSO_4$] in two different frequency ranges, between 1800 and 400 cm^{-1} and 3200 and 2700 cm^{-1}. Data illustrate that IL/MOF composite presents new peaks that were not present in the pristine MOF. These newly formed peaks at 1226, 1061, 1016, and 740 cm^{-1} were also observed in the spectrum of the bulk [BMIM][$MeSO_4$], indicating the successful IL incorporation into the framework.[31–34] Among these bands, those at 1226 and 1016 were assigned to —SO_3 stretching in IL's anion (asymmetric ν_{as}(—SO_3) and symmetric ν_s(—SO_3) modes, respectively).[41,42] Although ν_{as}(—SO_3) did not show any significant shift higher than the spectral resolution, the symmetric mode ($\nu_s(SO_3)$) showed a blue shift of approximately 6 cm^{-1} upon incorporation into MOF. The symmetric stretching vibration of S—O (ν_s(S—O)) showed a blue shift of 6 cm^{-1}, from 734 cm^{-1} in the bulk IL to 740 cm^{-1} in the composite.[43] These shifts to higher frequencies imply the strengthening of the corresponding bonds in the IL's anion, showing the existence of a direct interaction between the MOF and the anion of IL.[31–34]

On the other hand, both the pristine MOF and the composite material exhibited the characteristic vibrational bands in the

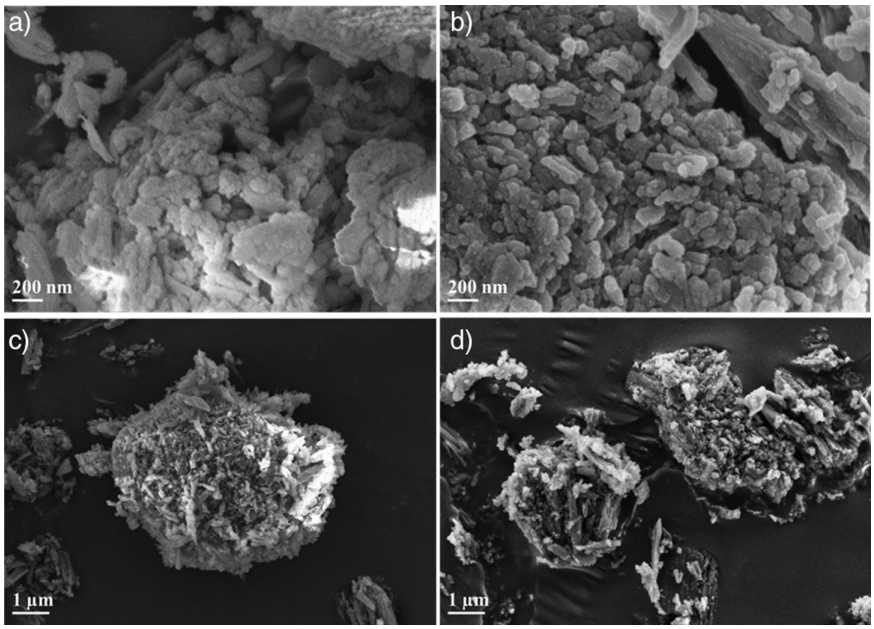

Figure 1. SEM micrographs of a,c) MIL-53(Al) and b,d) [BMIM][$MeSO_4$]/MIL-53(Al) at a magnification of 100 K× (a,b) and 25 K× (c,d). Sharpness enhanced image of (a) is given in Figure S2, Supporting Information.

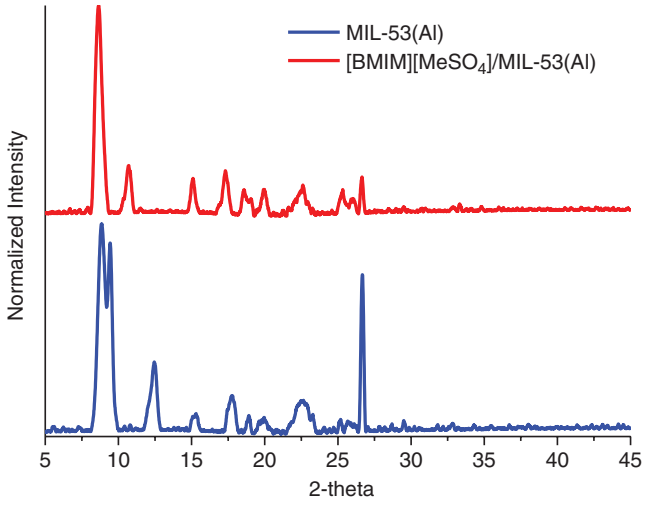

Figure 2. X-ray diffraction patterns of MIL-53(Al) (blue) and [BMIM][$MeSO_4$]/MIL-53(Al) (red).

1700–1400 cm^{-1} region for Al-coordinating carboxylate groups of terephthalic acid linker.[44,45] In addition, no additional bands could be observed in the 1700–1400 cm^{-1} region, indicating that there are no free linker molecules enclosed within the pores.[44] The asymmetric mode of —CO_2 stretching vibrations (ν_{as}(—CO_2)) was observed at 1603 and 1505 cm^{-1}, whereas the symmetric mode of carboxylic groups (ν_s(—CO_2)) was located at 1450 and 1418 cm^{-1} for pristine MIL-53(Al).[44] When the IR spectra of the pristine and the IL-incorporated MOF were compared, both symmetric —CO_2 stretching vibrations showed slight red shifts from 1450 and 1418 to 1447 and 1415 cm^{-1}, respectively, whereas the band assigned to stretching vibration between the carboxyl group and aromatic ring (ν(—CC)) shows a blue shift from 1163 to 1169 cm^{-1}. Two features located at 991 and 852 cm^{-1} also exhibited red shifts of 15 and 4 cm^{-1} upon IL incorporation, indicating a decrease in the energy of rocking vibration of the hydroxyl group (δ(—OH)) and bending vibration of the carboxyl group (δ(—CO_2)) or the aromatic ring (δ(—CCC)), respectively.[45] In addition, aluminum-oxide backbone, which is the secondary building unit of MIL-53(Al), can be a good indicator of interactions between the MOF and incorporated IL. Two features located at 681 and 658 cm^{-1} belong to asymmetric and symmetric stretches of aluminum-oxide backbone (ν(Al—O—Al)) in the IR spectrum of MIL-53(Al)[45] shifted to 696 and 662 cm^{-1}, respectively. These blue shifts indicate a possible strengthening of the aluminum-oxide backbone. Similarly, we also observed shifts in the high wavenumber region. The assignments for ν(C2H) and ν(HC4C5H) on the ring structure of IL's cation observed at 3104 and 3152 cm^{-1} exhibited blue shifts of 40 and 11 cm^{-1}, respectively.[46] Along with these major shifts, other peak assignments for pristine and IL-incorporated MIL-53(Al) are given in Table S1, Supporting Information. Consequently, as we observed major shifts in the bands assigned to IL and aluminum-oxide backbone, it can be inferred that the ions of the incorporated IL interacted with the MOF in the composite. Since polar molecules such as CO_2 interact mainly with hydroxyl groups of pristine MIL-53(Al),[47] it is assumed that IL, which is also a polar molecule, might interact with hydroxyl group of MIL-53(Al). Based on all these shifts discussed earlier, we deduce that $[MeSO_4]^-$ interacts with the hydroxyl groups in the MOF by weakening the corresponding bonds, which results in the strengthening of aluminum-oxide backbone, and weakening the carboxyl group of the linker molecules as evidenced by enhancing the strength of bond between the carboxyl group and the aromatic ring. This interaction may be the result of a repulsive interaction in a confined space or as a result of the interaction with positively charged sites

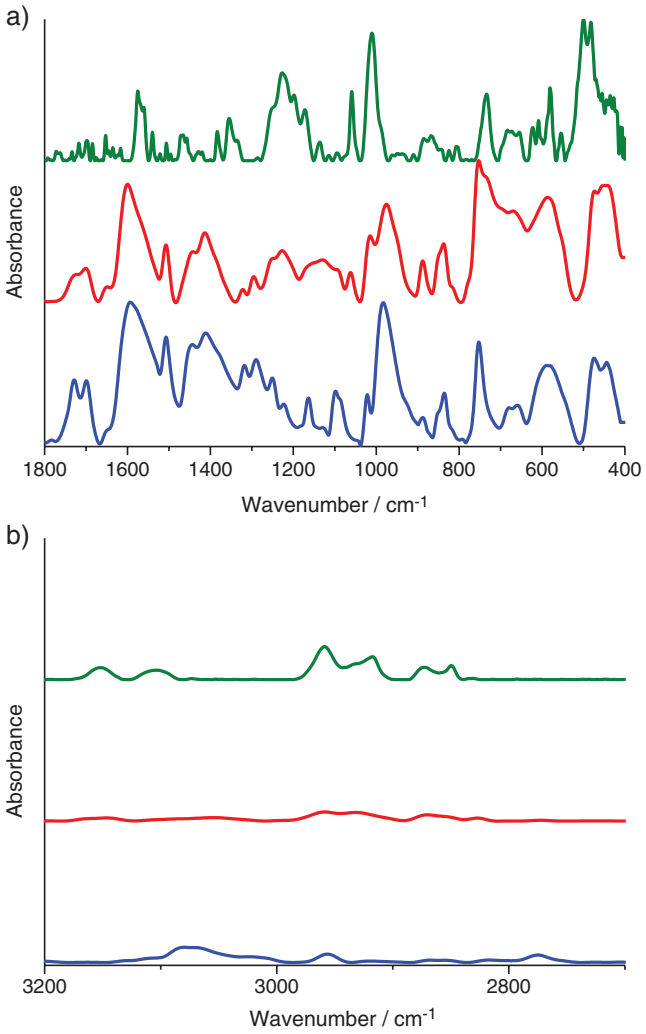

Figure 3. FTIR spectra of pristine MIL-53(Al) (blue), bulk [BMIM][$MeSO_4$] (green), and [BMIM][$MeSO_4$]/MIL-53(Al) (red) samples between a) 1800 and 400 cm^{-1} and b) 3200 and 2700 cm^{-1}.

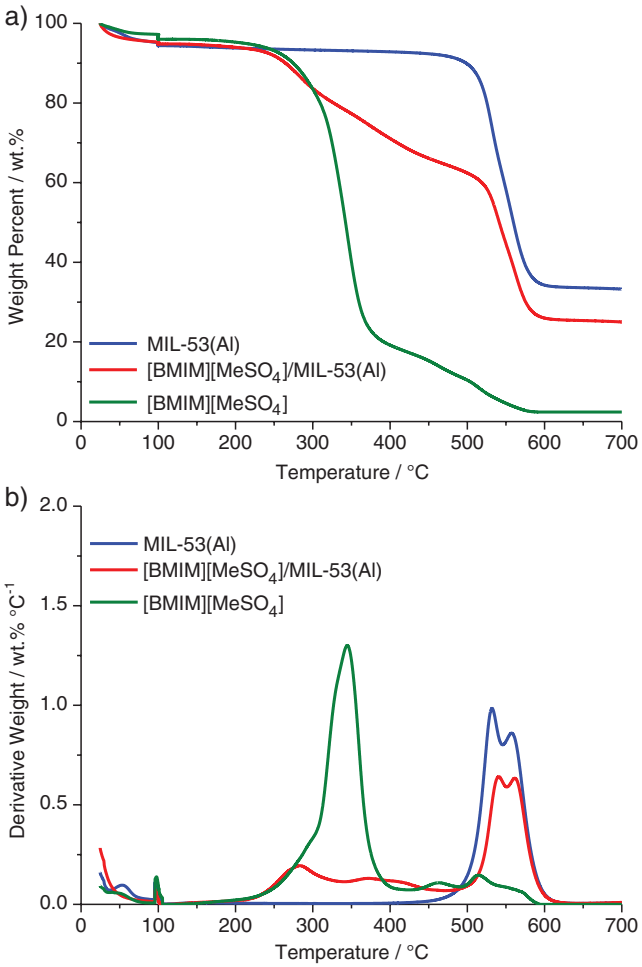

Figure 4. a) TGA and b) DTG curves of pristine MIL-53(Al) (blue), bulk [BMIM][$MeSO_4$] (green), and [BMIM][$MeSO_4$]/MIL-53(Al) (red) samples.

Table 2. Derivative onset temperature (T'_{onset}) and weight loss of pristine MIL-53(Al), bulk [BMIM][$MeSO_4$], and [BMIM][$MeSO_4$]/MIL-53(Al) samples.

Sample	T'_{onset} [°C]	Weight loss [wt%]
MIL-53(Al)	498	66
[BMIM][$MeSO_4$]	257	97
[BMIM][$MeSO_4$]/MIL-53(Al)	235	76

(mainly aluminum sites) affecting the rest of the MOF structure. The interaction of the IL's anion with MOF also improves the strength of inner S—O bond, signified by blue shifts in ν_s(—SO_3). When the interaction between the MOF and anion of IL increases, interionic interaction of IL weakens as implied by a blue shift in ν(C2H).[48] As a result, these interactions in the composite material should have a significant influence on the thermal stability limits and gas uptake amounts.

Thermogravimetric analysis (TGA) results of the pristine MIL-53(Al), bulk [BMIM][$MeSO_4$], and [BMIM][$MeSO_4$]/MIL-53(Al) are shown in **Figure 4**. The derivative onset temperature (T'_{onset}) of the IL-incorporated MIL-53(Al) was found as 235 °C, whereas that of the pristine MOF and bulk IL were 498 and 257 °C, respectively, as stated in **Table 2**. TGA of the samples in Figure 4 further indicated that the thermal decomposition of IL-incorporated MIL-53(Al) occurs by more than one step unlike pristine MOF and bulk IL. After the removal of water content, first decomposition starts at 235 °C, which is 22 °C lower than the decomposition temperature of bulk IL, and continues with a constant rate until the second decomposition step begins at 511 °C, which is 13 °C higher than that of pristine MIL-53(Al). This change in the decomposition mechanism provides evidence on the existence of direct interactions between MIL-53(Al) and [BMIM][$MeSO_4$], as indicated by the FTIR results. Eventually, the individual thermal decomposition reactions vary significantly because the IL-incorporated MIL-53(Al) behaves as a different system because of these interactions.

To investigate the effects of these interactions between MIL-53(Al) and [BMIM][$MeSO_4$] on the performance of the

composite material, we performed volumetric CH_4, CO_2, and N_2 adsorption measurements at 25 °C up to 5 bar. **Figure 5** shows the adsorption isotherms of these gases on the IL/MOF composite in comparison with those of pristine MOF.

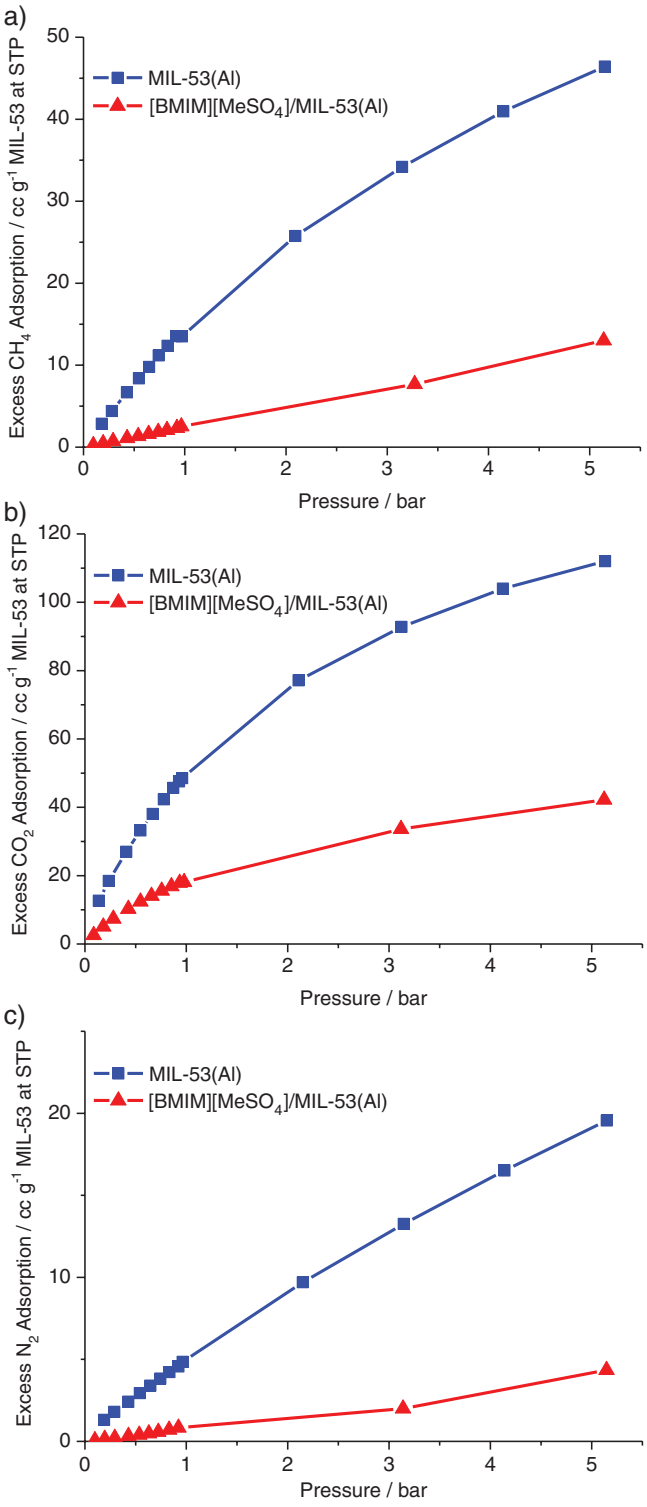

Figure 5. Excess adsorption isotherms of a) CH_4, b) CO_2, and c) N_2 in pristine MIL-53(Al) and [BMIM][$MeSO_4$]/MIL-53(Al) at 25 °C.

As BET and XRF measurements confirmed that the available pore volume and number of adsorption sites decrease, the IL/MOF composite has lower gas uptakes compared with pristine MOF.[31–34] However, data suggest that each gas shows a different level of decrease in uptake. These can be attributed to the differences in the interactions between the guest molecules and the IL/MOF composite, in which the IL interacts strongly with the adsorption sites of the MIL-53(Al), as indicated by the FTIR and TGA results. The different level of decrease in gas adsorption performance offers opportunities for improving the gas separation performance of materials. Therefore, we fitted excess gas adsorption isotherms to dual-site Langmuir models and calculated ideal selectivities of pristine and IL-incorporated MIL-53(Al). Isotherm fitting parameters are provided in Table S2 and S3, Supporting Information.

Figure 6 shows ideal selectivities of pristine MIL-53(Al) and [BMIM][$MeSO_4$]/MIL-53(Al) for CO_2/CH_4 and CO_2/N_2 separations at 25 °C and up to 5 bar. Since CO_2 strongly interacts with hydroxyl groups of MIL-53(Al)[37,49] and it has a higher solubility

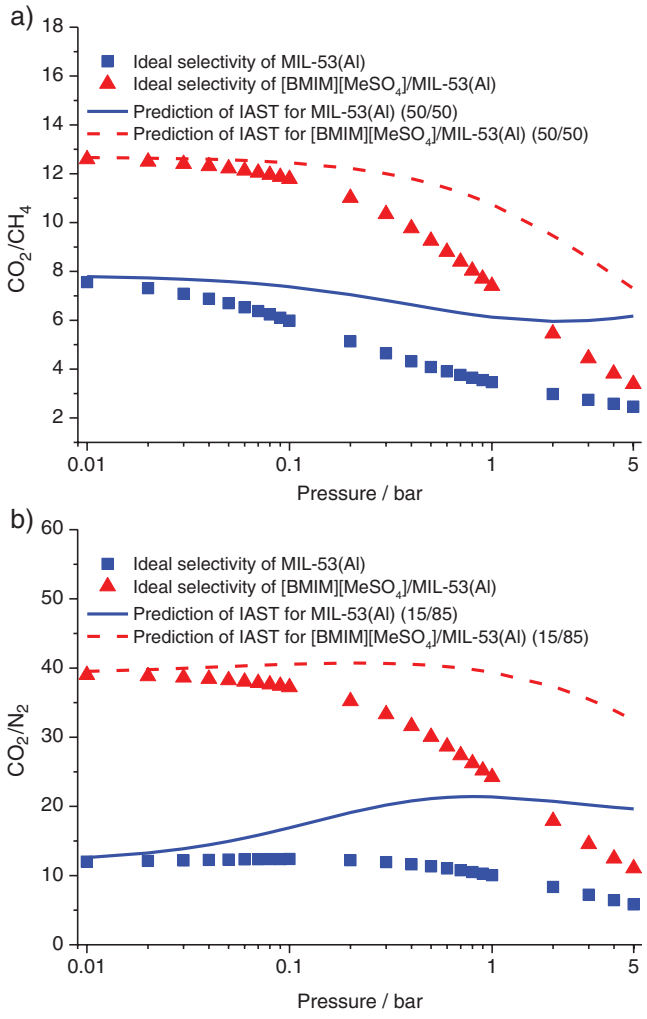

Figure 6. Ideal and mixture (for CO_2/CH_4:50/50 and for CO_2/N_2:15/85) selectivities of MIL-53(Al) and [BMIM][$MeSO_4$]/MIL-53(Al) samples for a) CO_2/CH_4 and b) CO_2/N_2 separations at 25 °C.

in [BMIM][$MeSO_4$],[38] higher adsorption was observed for CO_2 in both pristine and IL-incorporated MIL-53(Al) compared with other gases. As a result, CO_2/CH_4 and CO_2/N_2 selectivities of MIL-53(Al) were enhanced upon IL incorporation. The CO_2/CH_4 selectivity of the IL/MOF composite exhibits an approximately two times increase compared with pristine MIL-53(Al) up to 1 bar (Figure 6a). The most remarkable improvement was obtained in the CO_2/N_2 selectivity of the IL/MOF composite. Data showed that the improvement was more than three times at low pressures up to 0.1 bar, and it was approximately two times higher up to 5 bar (Figure 6b). The incorporation of [BMIM][$MeSO_4$] improves CO_2 selectivity of MIL-53(Al) and provides new opportunities for designing new composites with MIL-53(Al), an MOF that has not been considered before for IL/MOF composites, to the best of our knowledge.

Gases exist as mixtures in real separation processes; therefore, we predicted binary mixture gas adsorption isotherms in both pristine and IL-incorporated MIL-53(Al) samples, considering CO_2/CH_4:50/50 and CO_2/N_2:15/85 mixtures to represent natural gas and flue gas, respectively. We used ideal adsorption solution theory (IAST)[50] to obtain multicomponent adsorption isotherms using the data of single-component adsorption isotherms we measured. As shown in Figure 6, binary mixture selectivities (CO_2/CH_4:50/50 and CO_2/N_2:15/85) of pristine MOF and the IL/MOF composite predicted by the IAST were in good agreement with the ideal selectivities as pressure approach to zero as expected.[31] Selectivities for both CO_2/CH_4 and CO_2/N_2 mixtures were higher than the ideal selectivities at a high pressure as shown in Figure 6a,b, respectively. The selectivity of the IL/MOF composite was approximately 11 and 39 for CO_2/CH_4 and CO_2/N_2 mixtures, respectively, at 1 bar and 25 °C, which are almost twice of those of MIL-53(Al). This is an anticipated outcome as the single-component adsorption isotherms showed that CO_2 molecules are more strongly adsorbed than CH_4 and N_2 by pristine and IL-incorporated MIL-53(Al) so that they occupy more adsorption sites in the framework. As a consequence of this competitive adsorption between gases, higher mixture selectivities were obtained than ideal selectivities. Both ideal and mixture selectivities of the composite for CO_2/N_2 separation were improved three-times in comparison with pristine MIL-53(Al) at low pressures, also showing higher CO_2/N_2 selectivity than the recently reported data for postsynthetically modified MIL-101.[51]

To further understand the reasons of improved CO_2 separation performance of the composite, we measured the isosteric heat of adsorption (Q_{st}) values of CO_2, CH_4, and N_2 as a function of gas uptake in MIL-53(Al) and [BMIM][$MeSO_4$]/MIL-53(Al). Q_{st} values of CO_2, CH_4, and N_2 in MIL-53(Al) that we measured were found to be in good agreement with the literature.[52,53] Data given in **Figure 7** illustrate that the Q_{st} of CO_2 in [BMIM][$MeSO_4$]/MIL-53(Al) composite is higher than that in pristine MIL-53(Al), whereas the Q_{st} values of CH_4 and N_2 in [BMIM][$MeSO_4$]/MIL-53(Al) are lower than those in MIL-53(Al) throughout the whole uptake range. Results indicate stronger interactions between CO_2 and MIL-53(Al) upon IL incorporation, which is consistent with our findings showing improved CO_2/CH_4 and CO_2/N_2 selectivities of IL-incorporated MIL-53(Al).

For industrial applications, the reusability of the material is another important parameter. Hence, we performed cyclic

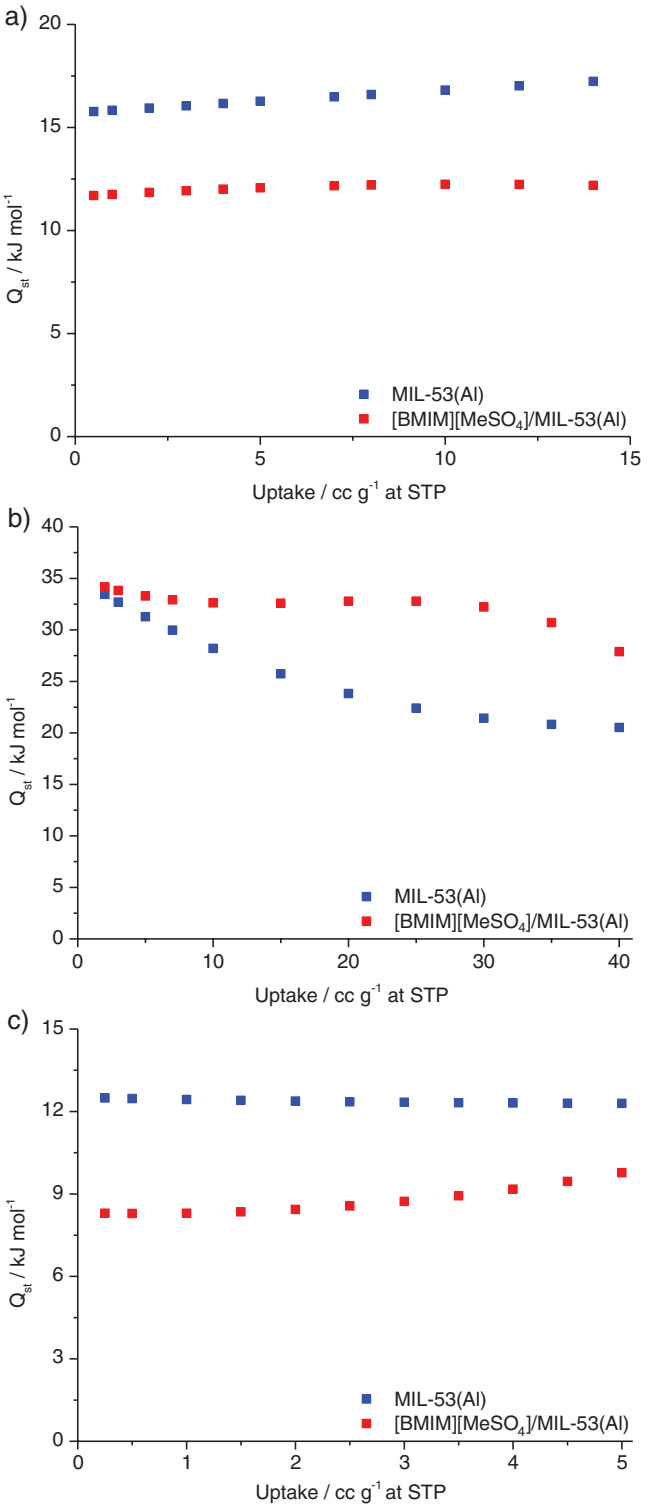

Figure 7. Isosteric heat of adsorption values of a) CH_4, b) CO_2, and c) N_2 in MIL-53(Al) and [BMIM][$MeSO_4$]/MIL-53(Al).

CO_2 adsorption measurements on the composite material under ideal conditions using a different batch of sample prepared by the same procedure. **Figure 8** shows that CO_2 adsorption capacity of

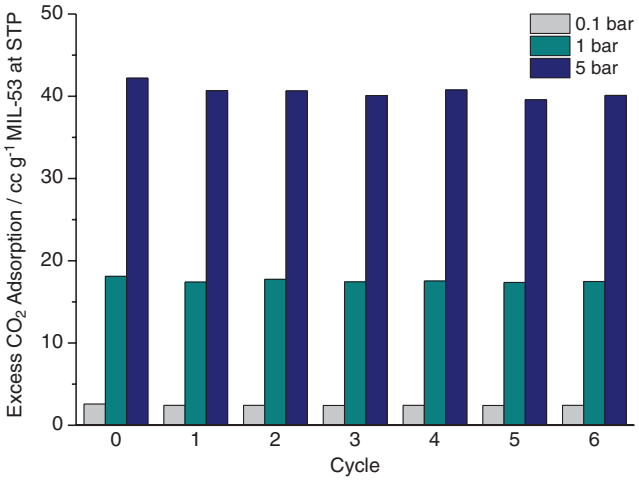

Figure 8. CO_2 adsorption capacity of [BMIM][$MeSO_4$]/MIL-53(Al) during six cycles at 25 °C. Bars indicated as 0 represent the first synthesized batch, and the other six represent the consecutive adsorption cycles of the different batch synthesized with the same procedure.

[BMIM][$MeSO_4$]/MIL-53(Al) composite remained very stable during six cycles. Data further showed that there is no hysteresis between adsorption and desorption isotherms for CO_2 (the cyclic CO_2 adsorption–desorption data are provided in Figure S4, Supporting Information). These results indicate that there is no IL leaching and the sample is reusable. Based on these enhancements in CO_2 selectivities and readiness for reuse, [BMIM][$MeSO_4$]/MIL-53(Al) composite can be accepted as a promising alternative in CO_2 separation processes.

3. Conclusion

This study illustrates that [BMIM][$MeSO_4$] incorporation with a loading of 26 wt% into MIL-53(Al) significantly improves the CO_2 selectivity of the parent MOF over CH_4 and N_2. Detailed characterizations of pristine and [BMIM][$MeSO_4$]-incorporated MIL-53(Al) samples were investigated by XRF, BET, SEM, XRD, FTIR, and TGA measurements. XRF and BET results showed the successful incorporation of [BMIM][$MeSO_4$] into the MOF. SEM and XRD results confirmed the stability of MIL-53(Al) upon the IL incorporation, whereas FTIR showed the evidence on the existence of direct interactions between the MOF and the confined IL. Results from TGA indicated that these interactions change the decomposition mechanism of the composite material compared with pristine MOF and bulk IL. Volumetric gas adsorption measurements illustrated a decrease in the uptake of each gas at different levels upon the IL incorporation. The IL/MOF composite showed the highest affinity toward CO_2 over CH_4 and N_2 up to 5 bar. As a result, the ideal CO_2/CH_4 selectivity increased from 4.1 to 9.3 at 0.5 bar, and ideal selectivity for CO_2/N_2 improved from 12 to 39 at 0.01 bar. Results further demonstrated that IL incorporation doubles the CO_2/N_2 selectivity of MIL-53(Al) even at relatively higher pressures, up to 5 bar. Similarly, IAST calculations showed that IL incorporation doubles CO_2/CH_4:50/50 and CO_2/N_2:15/85 mixture selectivities compared with those of parent MOF at 1 bar. The heat of adsorption results indicated that Q_{st} of CO_2 increased while those of CH_4 and N_2 decreased upon the incorporation of the IL, and consequently, the composite becomes more selective toward CO_2. All these results indicate that the novel composite material we introduced in this study has a strong potential to be used for the efficient separation of CO_2 from natural gas and flue gas. Finally, our results suggest that the IL/MOF composites having enhanced gas separation performances can be designed by altering the possible combinations of ILs and MOFs with an almost limitless number of possibilities.

4. Experimental Section

Materials: MIL-53(Al) (Basolite A100, aluminum terephthalate), [BMIM][$MeSO_4$] (1-*n*-butyl-3-methylimidazolium methyl sulfate), and acetone (≥99.5%) were obtained from Sigma–Aldrich and stored in glove box (Protector Controlled Atmosphere, Labconco) filled with Ar gas. CO_2 (99.9%), N_2 (99.998%), and He (99.999%) gases were obtained from Air Liquide, and CH_4 (99.95%) gas was purchased from Messer Group for the gas adsorption measurements.

Sample Preparation: We first activated MIL-53(Al) at 200 °C overnight under vacuum, and IL-incorporated MIL-53(Al) composite ([BMIM][$MeSO_4$]/MIL-53(Al)) was prepared using the method as reported earlier.[31] Earlier studies showed that as the IL loading increases, better gas separation performances were obtained, therefore the maximum achievable IL loading that does not result in a mud formation when mixed with MOF was used in this work. We dissolved [BMIM][$MeSO_4$] (300 mg) in acetone (20 mL) by stirring at ambient conditions for 1 h. Then, the dehydrated MIL-53(Al) (700 mg) was added while stirring the mixture at 35 °C. After the acetone was almost completely evaporated, we dried the sample at 105 °C overnight and stored in a desiccator.

XRF Spectroscopy: The elemental analyses of the samples were performed on a Bruker S8 Tiger spectrometer. X-ray tube with 4 kW Rh anode was used for the XRF analyses carried out under helium atmosphere.

BET Surface Area and Pore Analysis: The BET analyses were conducted on a Micromeritics ASAP 2020 BET Analyzer (Micromeritics) using 150 mg of sample. After the activation of samples at 150 °C overnight under vacuum, N_2 gas adsorption isotherms were obtained at 77 K. Surface areas were determined using the BET equation, and the pore volumes of the samples were obtained by the *t*-plot method.

Scanning Electron Microscopy: SEM images were taken using a Zeiss Evo LS 15 with an accelerating voltage of 3 kV and a working distance of 6.5 mm under vacuum. Morphological analyses of the surface of pristine MIL-53(Al) and [BMIM][$MeSO_4$]/MIL-53(Al) were done at 25 K× and 100 K×.

XRD Spectroscopy: XRD patterns were collected by using a Bruker D8 phaser instrument with a Cu Kα_1 ($\lambda = 1.5406$ Å) radiation source and Lynxeye detector. Generator at 10 mA of current and 30 kV of voltage was used with a resolution of 0.0204° between 5° and 45°.

FTIR Spectroscopy: A Bruker Vertex 80v FTIR spectrometer was used for IR spectroscopy. Analyses were conducted using potassium bromide (KBr) windows as the sample holder under vacuum at room temperature. Five hundred and twelve (128) scans were performed for sample (background) scan between the range of 4000 and 400 cm^{-1} in the transmission mode. The resolution of 2 cm^{-1} was used for each measurement.

Thermogravimetric Analysis: TGA curves were collected using a TA Instruments Q500 thermogravimetric analyzer. For pristine MIL-53(Al), bulk [BMIM][$MeSO_4$], and [BMIM][$MeSO_4$]/MIL-53(Al) composite, the following procedure was applied using a platinum sample pan. The temperature was first increased to 100 °C at a heating rate of 5 °C min^{-1}, and an isothermal condition was maintained for 8 h. After that, a ramp rate of 2 °C min^{-1} was applied until the temperature reached to 700 °C. During the measurements, continuous N_2 flow was provided for balance and purged with a rate of 40 and 60 mL min^{-1}, respectively. Thermal

decomposition temperatures were determined from the derivative thermogravimetric (DTG) curve as the derivative onset temperature (T'_{onset}) because they are generally overestimated by the onset temperature (T_{onset}).[54]

Gas Adsorption Measurements: Gas adsorption performances of pristine MIL-53(Al) and IL/MOF composite were measured using a High Pressure Volumetric Adsorption analyzer (HPVA II Micromeritics). 350 mg of sample was used for each measurement. Before the analyses, we first activated both pristine MIL-53(Al) and [BMIM][$MeSO_4$]/MIL-53(Al) overnight at 150 °C under vacuum. The degassing treatment was completed when the pressure reached to 10^{-3} mbar. To remove residual gases, all lines were purged with He gas just before the analyses. We conducted the adsorption measurements of CO_2, CH_4, and N_2 gases on both pristine MOF and composite material at pressures in the range from 0.1 to 5 bar at a constant temperature of 25 °C. When the measurement was completed, dry weights of the samples were recorded, and these values were used to calculate gas adsorption amounts per gram of material. The dual-site Langmuir models were fitted to the adsorption isotherms using Ideal Adsorbed Solution Theory (IAST)++ software.[50] Ideal selectivities were calculated using the single-component gas adsorption isotherms, and mixture selectivities were estimated using the IAST.[50] The isosteric heat of adsorption (Q_{st}) values was evaluated by the virial method.[33] The adsorption of CO_2 on pristine MOF and the composite material was measured at two different temperatures (10 and 15 °C). The virial-type thermal adsorption equation was used to fit uptake values. (Fit parameters are provided in Table S4, Supporting Information). The reusability of the composite was investigated by CO_2 adsorption cycles for six-times.

Supporting Information

Supporting Information is available from the Wiley Online Library or from the author.

Acknowledgements

H.K, H.M.P., and S.K. contributed equally to this work. This study is supported by Koç University Seed Fund Program and by the Scientific and Technological Research Council of Turkey (TUBITAK) (project number: 114R093). Authors are grateful for the support of KUTEM (Koç University TÜPRAŞ Energy Center) and KUYTAM (Koç University Surface Science and Technology Center). A.U. acknowledges TUBA-GEBIP Award and TARLA for their support in cooperative research. S. K. acknowledges ERC-2017-Starting Grant. This research has received funding from the European Research Council (ERC) under the European Union's Horizon 2020 research and innovation programme (ERC-2017-Starting Grant, grant agreement no. 756489-COSMOS).

Conflict of Interest

The authors declare no conflict of interest.

Keywords

CO_2 separation, ionic liquids, metal organic frameworks

Received: February 5, 2019
Revised: March 19, 2019
Published online: May 9, 2019

[1] M. Abu Ghalia, Y. Dahman, *Energy Technol.* **2017**, *5*, 356.
[2] S. Keskin, D. S. Sholl, *Energy Environ. Sci.* **2010**, *3*, 343.
[3] C. Song, Q. Liu, N. Ji, S. Deng, J. Zhao, Y. Li, Y. Song, H. Li, *Renewable Sustainable Energy Rev.* **2018**, *82*, 215.
[4] Z. H. Yuan, M. R. Eden, R. Gani, *Ind. Eng. Chem. Res.* **2016**, *55*, 3383.
[5] J. Jiang, S. I. Sandler, *J. Am. Chem. Soc.* **2005**, *127*, 11989.
[6] N. Gilani, J. T. Daryan, A. Rashidi, M. R. Omidkhah, *Appl. Surf. Sci.* **2012**, *258*, 4819.
[7] K. Ahmad, O. Mowla, E. M. Kennedy, B. Z. Dlugogorski, J. C. Mackie, M. Stockenhuber, *Energy Technol.* **2013**, *1*, 345.
[8] B. Yao, S. Mandrà, J. O. Curry, S. Shaikhutdinov, H.-J. Freund, J. Schrier, *ACS Appl. Mater. Interfaces* **2017**, *9*, 43061.
[9] S. Cavenati, C. A. Grande, A. E. Rodrigues, *Sep. Sci. Technol.* **2005**, *40*, 2721.
[10] G. Férey, C. Mellot-Draznieks, C. Serre, F. Millange, *Acc. Chem. Res.* **2005**, *38*, 217.
[11] H. L. Li, M. Eddaoudi, M. O'Keeffe, O. M. Yaghi, *Nature* **1999**, *402*, 276.
[12] S. T. Meek, J. A. Greathouse, M. D. Allendorf, *Adv. Mater.* **2011**, *23*, 249.
[13] H. Furukawa, K. E. Cordova, M. O'Keeffe, O. M. Yaghi, *Science* **2013**, *341*, 1230444.
[14] H.-C. Zhou, J. R. Long, O. M. Yaghi, *Chem. Rev.* **2012**, *112*, 673.
[15] J. R. Li, R. J. Kuppler, H. C. Zhou, *Chem. Soc. Rev.* **2009**, *38*, 1477.
[16] A. O. Yazaydin, R. Q. Snurr, T. H. Park, K. Koh, J. Liu, M. D. LeVan, A. I. Benin, P. Jakubczak, M. Lanuza, D. B. Galloway, J. J. Low, R. R. Willis, *J. Am. Chem. Soc.* **2009**, *131*, 18198.
[17] A. Al-Mamoori, A. Krishnamurthy, A. A. Rownaghi, F. Rezaei, *Energy Technol.* **2017**, *5*, 834.
[18] Z. Zhang, Z. Z. Yao, S. Xiang, B. Chen, *Energy Environ. Sci.* **2014**, *7*, 2868.
[19] D. N. Dybtsev, H. Chun, K. Kim, *Chem. Commun.* **2004**, *14*, 1594.
[20] L. Peng, J. Zhang, J. Li, B. Han, Z. Xue, G. Yang, *Chem. Commun.* **2012**, *48*, 8688.
[21] E. R. Parnham, R. E. Morris, *Acc. Chem. Res.* **2007**, *40*, 1005.
[22] S. Zhang, J. Sun, X. Zhang, J. Xin, Q. Miao, J. Wang, *Chem. Soc. Rev.* **2014**, *43*, 7838.
[23] M. Babucci, C.-Y. Fang, A. S. Hoffman, S. R. Bare, B. C. Gates, A. Uzun, *ACS Catal.* **2017**, *7*, 6969.
[24] A. Jalal, A. Uzun, *J. Catal.* **2017**, *350*, 86.
[25] B. Monteiro, A. R. Nabais, F. A. Almeida Paz, L. Cabrita, L. C. Branco, I. M. Marrucho, L. A. Neves, C. C. L. Pereira, *Energy Technol.* **2017**, *5*, 2158.
[26] E. D. Bates, R. D. Mayton, I. Ntai, J. H. Davis, *J. Am. Chem. Soc.* **2002**, *124*, 926.
[27] D. J. Tempel, P. B. Henderson, J. R. Brzozowski, R. M. Pearlstein, H. Cheng, *J. Am. Chem. Soc.* **2008**, *130*, 400.
[28] Y. Ban, Z. Li, Y. Li, Y. Peng, H. Jin, W. Jiao, A. Guo, P. Wang, Q. Yang, C. Zhong, W. Yang, *Angew. Chem., Int. Ed.* **2015**, *54*, 15483.
[29] M. Mohamedali, H. Ibrahim, A. Henni, *Chem. Eng. J.* **2018**, *334*, 817.
[30] M. Ding, H. Jiang, *ACS Catal.* **2018**, *8*, 3194.
[31] F. P. Kinik, C. Altintas, V. Balci, B. Koyuturk, A. Uzun, S. Keskin, *ACS Appl. Mater. Interfaces* **2016**, *45*, 30992.
[32] K. B. Sezginel, S. Keskin, A. Uzun, *Langmuir* **2016**, *4*, 1139.
[33] B. Koyuturk, C. Altintas, F. P. Kinik, S. Keskin, A. Uzun, *J. Phys. Chem. C* **2017**, *121*, 10370.
[34] V. Nozari, S. Keskin, A. Uzun, *ACS Omega* **2017**, *10*, 6613.
[35] M. Zeeshan, V. Nozari, M. B. Yagci, T. Isık, U. Unal, V. Ortalan, S. Keskin, A. Uzun, *J. Am. Chem. Soc.* **2018**, *140*, 10113.
[36] B. C. R. Camacho, R. P. P. L. Ribeiro, I. A. A. C. Esteves, J. P. B. Mota, *Sep. Purif. Technol.* **2014**, *141*, 150.
[37] S. Bourrelly, P. L. Llewellyn, C. Serre, F. Millange, T. Loiseau, G. Férey, *J. Am. Chem. Soc.* **2005**, *127*, 13529.
[38] J. Kumełan, Á. Pérez-Salado Kamps, D. Tuma, G. Maurer, *J. Chem. Eng. Data* **2006**, *51*, 1802.

[39] J. D. Holbrey, W. M. Reichert, R. P. Swatloski, G. A. Broker, W. R. Pitner, K. R. Seddonb, R. D. Rogersa, *Green Chem.* **2002**, *4*, 407.
[40] J. Liu, F. Zhang, X. Zou, G. Yu, N. Zhao, S. Fan, G. Zhu, *Chem. Commun.* **2013**, *49*, 7430.
[41] Q. Zhang, N. Wang, Z. Yu, *J. Phys. Chem. B* **2010**, *114*, 4747.
[42] J.-M. Andanson, M. Traïkia, P. Husson, *J. Chem. Thermodyn.* **2014**, *77*, 214.
[43] A. Borba, A. Gómez-Zavaglia, P. N. N. L. Simões, R. Fausto, *Spectrochim. Acta A* **2005**, *61*, 1461.
[44] T. Loiseau, C. Serre, C. Huguenard, G. Fink, F. Taulelle, M. Henry, T. Bataille, G. Férey, *Chem. Eur. J.* **2004**, *10*, 1373.
[45] A. E. J. Hoffman, L. Vanduyfhuys, I. Nevjestić, J. Wieme, S. M. J. Rogge, H. Depauw, P. Van Der Voort, H. Vrielinck, V. J. Van Speybroeck, *J. Phys. Chem. C* **2018**, *122*, 2734.
[46] T. Singh, A. Kumar, *Vib. Spectrosc.* **2011**, *55*, 119.
[47] N. A. Ramsahye, G. Maurin, S. Bourrelly, P. L. Llewellyn, C. Serre, T. Loiseau, T. Devic, G. Férey, *J. Phys. Chem. C* **2008**, *112*, 514.
[48] M. Babucci, A. Akçay, V. Balci, A. Uzun, *Langmuir* **2015**, *31*, 9163.
[49] M. Mihaylov, K. Chakarova, S. Andonova, N. Drenchev, E. Ivanova, E. A. Pidko, A. Sabetghadam, B. Seoane, J. Gascon, F. Kapteijn, K. Hadjiivanov, *Chem. Commun.* **2016**, *52*, 1494.
[50] S. Lee, J. H. Lee, J. Kim, *Korean J. Chem. Eng.* **2018**, *35*, 214.
[51] D. K. Yoo, N. A. Khan, S. H. Jhung, *J. CO2 Util.* **2018**, *28*, 319.
[52] P. Mishra, H. P. Uppara, B. Mandal, S. Gumma, *Ind. Eng. Chem. Res.* **2014**, *53*, 19747.
[53] J. Möllmer, M. Lange, A. Möller, C. Patzschke, K. Stein, D. Lässig, J. Lincke, R. Gläser, H. Krautscheid, R. Staudt, *J. Mater. Chem.* **2012**, *22*, 10274.
[54] A. Akçay, M. Babucci, V. Balci, A. Uzun, *Chem. Eng. Sci.* **2015**, *123*, 588.